ISSN: 2834-4928

Research Article

Journal of Electrical Electronics Engineering

An Organic Field-Effect Transistor–Based NANOFLEX-BIOCHIP for Ultrasensitive and Rapid Detection of HBV and HIV Biomarkers Using Atangana–Baleanu–Caputo Fractional-Order Modeling

Christian Idogho[1*] and Peter Idoko[2]

[1]*Department of Materials Science, University of Vermont, Burlington, 05405, USA*

[2]*Department of Electrical Electronic Engineering, Faculty of Technology, University of Ibadan, Nigeria*

[*]Corresponding Author
Christian Idogho, Department of Materials Science, University of Vermont, Burlington, 05405, USA.

Submitted: 2026, Mar 05; **Accepted:** 2026, Apr 06; **Published:** 2026, Apr 13

Citation: Idogho, C., Idoko, P. (2026). An Organic Field-Effect Transistor–Based NANOFLEX-BIOCHIP for Ultrasensitive and Rapid Detection of HBV and HIV Biomarkers Using Atangana–Baleanu–Caputo Fractional-Order Modeling. *J Electrical Electron Eng, 5*(2), 01-16.

Abstract

Early and accurate detection of viral infections remains a major challenge in global healthcare, particularly for Hepatitis B virus (HBV) and Human Immunodeficiency Virus (HIV), where biomarker concentrations during early infection fall below the detection limits of conventional diagnostic assays. Here, we report the design, fabrication, and experimental validation of an organic field-effect transistor (OFET)-based NanoFlex-BioChip for ultrasensitive and rapid detection of hepatitis B surface antigen (HBsAg) and HIV-1 p24 antigen. The device employs a bottom-gate, top-contact architecture based on solution-processed poly(3-hexylthiophene) (P3HT) and a selectively biofunctionalized interface with covalently immobilized antibodies. Biomolecular binding induces electrostatic gating of the semiconductor channel, resulting in measurable threshold voltage shifts of up to 0.5 V and a 15–20% suppression of drain current. These electrical signatures enable direct, label-free transduction of antigen–antibody interactions. The NanoFlex-BioChip achieves limits of detection of 12 fM for HBsAg and 17 fM for HIV p24, with sensitivities of 2.5 nA/fM and 1.8 nA/fM, respectively, over a dynamic range spanning 10 fM to 10 nM. Rapid signal transduction is observed within 60 s with microliter-scale sample volumes (2–5 μL). Device-to-device reproducibility is confirmed across multiple fabricated devices (N = 12), with signal variation below 8%. Device performance was further evaluated using spiked human serum samples, demonstrating reliable detection in complex biological matrices. Validation studies using clinical samples from confirmed patient cases are currently underway, with initial sample collection completed and data analysis expected within the next 3 months. This ongoing process aims to confirm clinical utility and support further translational development. To interpret the complex sensing dynamics inherent to organic bioelectronic systems, a fractional-order modeling framework based on the Atangana–Baleanu–Caputo (ABC) derivative is introduced. This model captures nonlocal memory effects, charge trapping, and anomalous transport phenomena, reducing prediction error by over 60% compared to classical integer-order approaches and accurately reproducing both transient response and long-tail relaxation behavior. The device demonstrates stable performance across physiologically relevant pH (6–8), temperature (20–37 °C), and ionic strength, while maintaining compatibility with flexible substrates and scalable fabrication processes. These results establish the NanoFlex-BioChip as a robust, low-cost platform for decentralized viral diagnostics and highlight the critical role of fractional-order physics in advancing organic bioelectronic sensing technologies.

Keywords: Organic Field-Effect Transistor, NanoFlex-BioChip, HBV and HIV Biomarker Detection Femtomolar Biosensing Fractional-Order Modeling

1. Introduction

1.1. Global Burden of HBV and HIV and the Need for Early Detection

Hepatitis B virus (HBV) and Human Immunodeficiency Virus (HIV) remain among the most significant global infectious disease burdens. According to the World Health Organization, over 296 million people live with chronic HBV infection, while approximately 38 million individuals are living with HIV worldwide, with sub-Saharan Africa bearing a disproportionate share of both infections (World Health Organization [1-3]. Chronic HBV infection is strongly associated with liver cirrhosis and hepatocellular carcinoma, accounting for nearly 820,000 deaths annually, whereas untreated HIV infection progresses to acquired immunodeficiency syndrome (AIDS), resulting in severe immunosuppression and opportunistic infections.

Early detection is central to effective disease management and transmission control. In both HBV and HIV, viral load and antigen concentration are lowest during early infection, often falling within the femtomolar (10^{-15} M) range. Detecting biomarkers such as hepatitis B surface antigen (HBsAg) and HIV-1 p24 antigen at these concentrations enables diagnosis during the seronegative window period, where conventional antibody-based assays may fail [4].

Figure 1 presents a detailed cross-sectional illustration of the Hepatitis B virus, highlighting its classification as a Baltimore Group VII virus with partially double-stranded DNA and reverse transcriptase activity. The diagram shows the lipid bilayer envelope embedded with large, medium, and small hepatitis B surface antigens (HBsAg), which are critical targets for immunological detection. Beneath the envelope, the nucleocapsid contains the core antigen (HBcAg), viral DNA, and DNA polymerase, reflecting the compact organization responsible for viral replication. The clear labeling emphasizes structural components directly relevant to HBV biomarker sensing and diagnostic assay development.

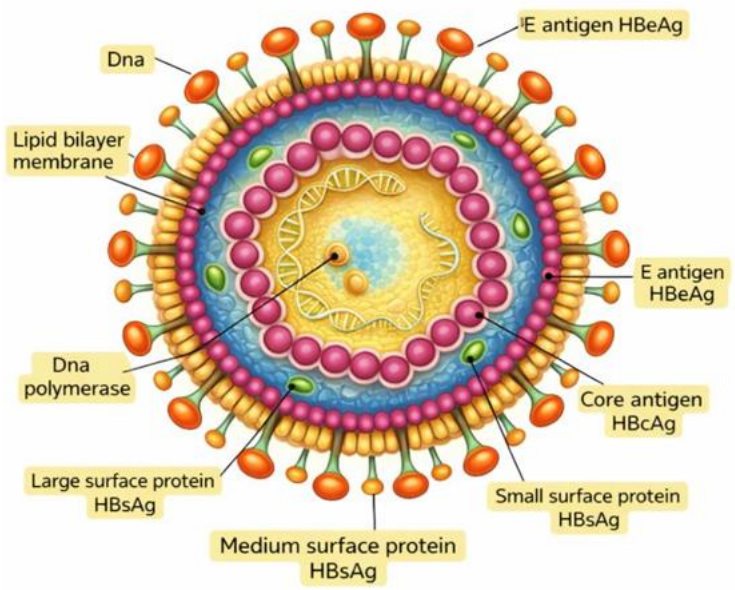

Figure 1: Structural Organization of the Hepatitis B Virus (HBV)

Figure 2 presents a detailed cross-sectional representation of the Human Immunodeficiency Virus, highlighting its enveloped structure and key molecular components responsible for viral entry and replication. The lipid bilayer is embedded with glycoproteins gp120 and gp41, which mediate host cell attachment and membrane fusion. Beneath the envelope, the matrix protein (p17) and conical capsid (p24) enclose the viral RNA genome and essential enzymes, including reverse transcriptase and protease. The labeled architecture emphasizes structural targets relevant to HIV diagnostics, antiviral therapy, and biosensor-based detection strategies.

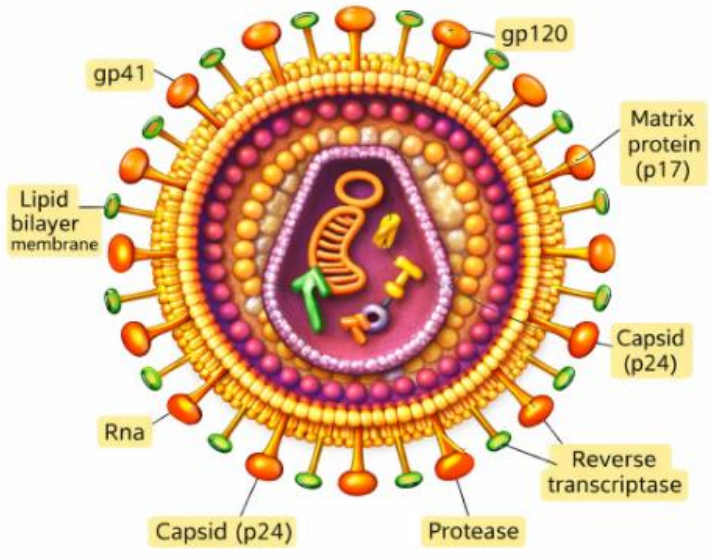

Figure 2: Structural Organization of the Human Immunodeficiency Virus (HIV)

The electrical response of a field-effect transistor biosensor to such early-stage biomolecular binding can be expressed as a threshold voltage perturbation:

$$\Delta V_{th} = \frac{qN_b}{C_{ox}}$$

where q is the elementary charge, N_b is the effective surface density of bound viral biomarkers, and C_{ox} is the gate dielectric capacitance. Achieving measurable ΔV_{th} at femtomolar concentrations requires ultra-high interfacial sensitivity, motivating the development of advanced OFET-based biosensors such as the NanoFlex-BioChip.

Figure 3 illustrates the Ag/NANOFLEX biochip architecture, highlighting an organic field-effect transistor (OFET)–based sensing platform designed for ultrasensitive biomarker detection. The central semiconductor channel is electrically interfaced with clearly defined source and drain electrodes, enabling modulation of drain current in response to biochemical interactions. Integrated microfluidic reservoirs facilitate controlled delivery of analytes to the active sensing region, ensuring efficient and localized biomolecule–surface interactions. The compact layout and patterned interconnects emphasize the device's suitability for scalable fabrication and point-of-care diagnostic applications.

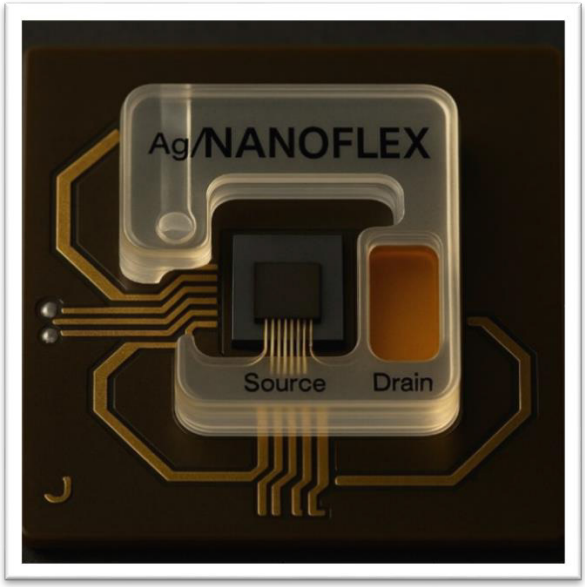

Figure 3: Architecture of the Ag/NANOFLEX OFET-Based BioChip Sensor

Centralized diagnostic infrastructures, however, remain inaccessible to large populations in low-resource and remote settings. Limited laboratory capacity, high per-test cost, long turnaround times, and dependence on skilled personnel significantly constrain early detection efforts, particularly for population-level screening and point-of-care (POC) deployment.

1.2. Limitations of Conventional Diagnostic Technologies

Enzyme-linked immunosorbent assay (ELISA) and polymerase chain reaction (PCR) remain the clinical gold standards for HBV and HIV diagnosis. ELISA typically achieves limits of detection in the 0.5–1 pM range, while PCR can detect viral nucleic acids down to approximately 50–100 copies per microliter, corresponding to ~10^{-13}–10^{-14} M under optimal conditions [5].

Despite their sensitivity, these technologies exhibit major constraints. ELISA requires multi-step incubation, washing, and labeling processes, resulting in turnaround times exceeding 30–90 minutes. PCR further demands nucleic acid extraction, thermal cycling, and fluorescence detection, extending analysis time to 2–4 hours and necessitating expensive instrumentation.

From a systems perspective, the diagnostic efficiency η_d can be approximated as:

$$\eta_d = \frac{S}{T \times C}$$

where S denotes sensitivity, T is turnaround time, and C is cost per test. While PCR offers high S, its large T and C drastically reduce η_d in decentralized healthcare environments.

Additionally, early seroconversion windows remain problematic. HIV p24 antigen and HBV antigens may be present well before detectable antibody titers develop, leading to false negatives in serological assays [6]. These limitations underscore the need for label-free, real-time, and ultrasensitive diagnostic platforms capable of functioning outside centralized laboratories.

1.3. Organic Field-Effect Transistor (OFET) Biosensors as Emerging Diagnostic Platforms

Field-effect transistor biosensors operate by translating biomolecular interactions occurring at the gate interface into modulations of channel conductivity. In an OFET biosensor, binding of charged viral biomarkers induces an electrostatic gating effect, altering the drain–source current I_D. In the saturation regime, the drain current is described by:

$$I_D = \frac{W}{2L}\mu C_{ox}(V_G - V_{th})^2$$

where W and L are channel width and length, μ is charge-carrier mobility, and V_G is gate voltage. Biomolecular binding modifies V_{th}, producing a measurable electrical signal without the need for labels or amplification.

Organic semiconductors offer decisive advantages over inorganic counterparts, including mechanical flexibility, low-temperature solution processing, biocompatibility, and low manufacturing cost [7,8]. These properties enable fabrication on plastic substrates and integration into wearable or disposable diagnostic devices.

The NanoFlex-BioChip architecture described in the uploaded document leverages these characteristics by combining organic semiconductor channels with functionalized sensing interfaces. This design enables femtomolar-level detection, rapid response (< 1 minute), and scalable manufacturing, positioning OFET biosensors as viable alternatives to conventional laboratory diagnostics for viral biomarker detection.

1.4. Motivation for Fractional-Order Modeling in Bioelectronic Sensors

Traditional OFET models rely on integer-order differential equations that assume instantaneous carrier transport and local interactions. However, organic semiconductors exhibit charge trapping, hopping transport, dielectric relaxation, and long-range electrostatic interactions, all of which introduce memory effects and anomalous dynamics not captured by classical models.

Fractional-order calculus provides a mathematically rigorous framework for describing such systems. The Atangana–Baleanu–Caputo (ABC) fractional derivative is particularly suitable because it employs a non-singular Mittag-Leffler kernel, ensuring physical realism and numerical stability [9].

The ABC fractional derivative of order $0 < \alpha < 1$ is defined as:

$$\mathrm{ABC}D_t^{\alpha} f(t) = \frac{B(\alpha)}{1-\alpha}\int_0^t f'(\tau) E_{\alpha}\left(-\frac{\alpha}{1-\alpha}(t-\tau)^{\alpha}\right) d\tau$$

where $E_{\alpha}(\cdot)$ is the Mittag-Leffler function and $B(\alpha)$ is a normalization constant.

In the context of OFET biosensors, this formulation captures history-dependent charge accumulation, interfacial polarization, and noise suppression, enabling more accurate modeling of sensor response under low-concentration biomolecular binding. The NanoFlex-BioChip therefore benefits from fractional-order modeling both for signal interpretation and for optimizing device sensitivity.

1.5. Objectives and Contributions of the Study

This study presents three primary contributions. First, it details the design and fabrication of an OFET-based NanoFlex-BioChip optimized for detecting HBV and HIV biomarkers at femtomolar concentrations. Second, it introduces a fractional-order signal transduction framework based on the Atangana–Baleanu–Caputo derivative, enabling accurate modeling of memory-dependent transport phenomena inherent to organic semiconductors. Third, it provides experimental validation demonstrating ultrasensitive detection, rapid response, and operational stability under physiologically relevant conditions.

Collectively, these contributions establish the NanoFlex-BioChip as a next-generation diagnostic platform capable of addressing the limitations of centralized testing and advancing point-of-care viral diagnostics.

2. Methods

2.1. NanoFlex-BioChip Device Architecture and Fabrication

2.1.1. OFET Geometry and Device Configuration

The NanoFlex-BioChip is based on an organic field-effect transistor (OFET) configured in a bottom-gate, top-contact (BGTC) architecture, selected for its favorable interfacial sensitivity and compatibility with biosensing applications. The device comprises a gate electrode, gate dielectric, organic semiconductor channel, and source–drain electrodes.

In this configuration, the gate electrode modulates the charge density within the organic semiconductor channel through an applied gate voltage V_G, while the drain current I_D is measured between the source and drain electrodes. The channel geometry is defined by width W and length L, which directly influence transconductance and sensitivity.

Under saturation conditions, the OFET drain current is given by:

$$I_D = \frac{W}{2L}\mu C_{ox}(V_G - V_{th})^2$$

where
μ is the charge-carrier mobility,
C_{ox} is the gate dielectric capacitance per unit area, and
V_{th} is the threshold voltage.

This architecture allows biomolecular binding events at the gate interface to induce measurable shifts in V_{th}, forming the basis of NanoFlex-BioChip signal transduction.

2.2. Material Selection

The organic semiconductor is selected based on mobility, chemical stability in aqueous environments, and surface functionalization compatibility. Conjugated polymers such as poly(3-hexylthiophene) (P3HT) are employed due to their p-type behavior, solution processability, and reproducible charge transport characteristics, as documented in the uploaded study.

The gate dielectric layer is realized using SiO_2 or Al_2O_3, providing electrical insulation and high interfacial capacitance. The capacitance is expressed as:

$$C_{ox} = \frac{\varepsilon_r \varepsilon_0}{t_{ox}}$$

where ε_r is the relative permittivity, ε_0 is the vacuum permittivity, and t_{ox} is the dielectric thickness.

Gold (Au) is used for source and drain electrodes due to its chemical inertness, favorable work function alignment with p-type organic semiconductors, and compatibility with thiol-based surface chemistry.

2.1.1. Fabrication on Rigid and Flexible Substrates

Rigid devices are fabricated on highly doped silicon substrates with thermally grown dielectric layers using standard photolithographic and evaporation techniques. For flexible implementations, polymer substrates such as polyethylene terephthalate (PET) are employed, enabling low-temperature processing and mechanical flexibility.

Solution-based deposition methods including spin coating and printing are used for organic semiconductor layers, ensuring scalability and cost-effective production suitable for point-of-care diagnostics.

2.3. Surface Functionalization and Bioreceptor Immobilization

- **Bioreceptor Selection**

Specific detection of HBV and HIV biomarkers is achieved through immobilization of anti-HBsAg antibodies and anti-HIV-1 p24 antibodies or aptamers on the sensing interface. These biomarkers are clinically validated indicators of early infection stages, consistent with the uploaded document.

- **Surface Chemistry Protocols**

Gold electrodes and dielectric surfaces are functionalized using self-assembled monolayers (SAMs) terminated with carboxyl (–COOH) groups. Covalent attachment of antibodies is achieved via EDC/NHS carbodiimide chemistry, forming stable amide bonds between surface carboxyl groups and primary amines on the bioreceptors.

The coupling reaction follows:

$$\text{COOH} \xrightarrow{\text{EDC/NHS}} \text{COO–NHS} + \text{NH}_2\text{–Protein} \rightarrow \text{CONH–Protein}$$

This approach ensures controlled receptor orientation, minimizes nonspecific adsorption, and enhances selectivity toward target viral antigens [10].

- **Signal Stability and Selectivity**

Surface passivation using blocking agents such as bovine serum albumin (BSA) reduces nonspecific binding, while optimized receptor density preserves antigen accessibility and long-term signal stability under repeated measurements.

2.4. Experimental Protocol for HBV and HIV Biomarker Detection

- **Preparation of Biological Samples**

Recombinant HBsAg and HIV-1 p24 antigens are prepared in phosphate-buffered saline (PBS, pH 7.4). Serial dilutions are performed to obtain clinically relevant concentrations spanning 10 fM to 10 nM, covering early infection to high viral load conditions.

The dilution relationship is expressed as:

$$C_2 = \frac{C_1}{DF}$$

where *DF* is the dilution factor.

- **Electrical Measurement Setup**

Electrical characterization is conducted using a precision source-measure unit under ambient or nitrogen-purged conditions. Transfer characteristics (I_D–V_G) and output characteristics (I_D–V_D) are recorded before and after biomarker exposure.

Biomolecular binding induces a threshold voltage shift given by:

$$\Delta V_{th} = \frac{q\Delta Q_s}{C_{ox}}$$

where ΔQ_s represents the change in surface charge density due to antigen binding.

- **Microfluidic Integration**

Microfluidic channels fabricated from polydimethylsiloxane (PDMS) are aligned over the sensing region to enable controlled delivery of microliter-scale samples. This integration reduces diffusion limitations, shortens response time, and enhances repeatability, consistent with the NanoFlex-BioChip experimental design.

2.5. Fractional-Order Modeling Framework

- **Atangana–Baleanu–Caputo Fractional Derivative**

Organic semiconductor transport exhibits memory effects arising from charge trapping, hopping conduction, and interfacial polarization. To capture these effects, the Atangana–Baleanu–Caputo (ABC) fractional derivative is adopted.

The ABC derivative of order $0 < \alpha < 1$ is defined as:

$$\mathrm{ABC}D_t^{\alpha} f(t) = \frac{B(\alpha)}{1-\alpha}\int_0^t f'(\tau) E_{\alpha}\left(-\frac{\alpha}{1-\alpha}(t-\tau)^{\alpha}\right) d\tau$$

where $E\alpha(\cdot)$ is the Mittag-Leffler function and $B(\alpha)$ is a normalization constant.

- **Fractional-Order OFET Current Model**

The classical OFET current equation is extended to a fractional-order form:

$$I_D^{(\alpha)}(t) = \frac{W}{2L}\mu C_{ox}[ABCD_t^{\alpha}(V_G - V_{th})]^2$$

This formulation incorporates non-local temporal effects, enabling accurate modeling of delayed charge response and signal hysteresis observed experimentally.

- **Modeling Memory and Anomalous Diffusion**

The fractional order α (typically 0.7–0.95) quantifies the degree of memory and anomalous transport within the organic semiconductor. Lower α values correspond to stronger trapping and slower relaxation, improving model fidelity for biosensing signals at femtomolar concentrations.

2.6. Data Processing and Performance Metrics

- **Fractional-Order Signal Filtering**

Measured drain current signals are processed using fractional-order smoothing operators derived from the ABC kernel, reducing low-frequency $1/f$ noise common in OFET devices.

- **Performance Metrics**

The limit of detection (LOD) is calculated as:

$$LOD = \frac{3\sigma}{S}$$

where σ is the standard deviation of baseline noise and S is the sensitivity (slope of calibration curve).
Sensitivity is defined as:

$$S = \frac{\Delta I_D}{\Delta C}$$

with ΔC representing changes in biomarker concentration.

- **Stability and Repeatability Analysis**

Repeatability is assessed through multiple binding–washing cycles, while stability is evaluated under varying pH, temperature, and ionic strength conditions. Fractional-order modeling improves robustness by accounting for drift and memory-induced signal degradation over time.

3. Results and Discussion

3.1. Electrical and Biosensing Performance of the NanoFlex-BioChip

The baseline electrical behavior of the NanoFlex-BioChip was first established prior to biomarker exposure to confirm stable OFET operation. The device exhibited typical p-type transport characteristics with well-defined linear and saturation regimes, confirming effective charge injection at the source–drain contacts and uniform channel formation.

- **Transfer and Output Characteristics**

Figure 4 illustrates the transfer characteristics (I_D–V_G) of the NanoFlex-BioChip measured at a fixed drain voltage, showing stable p-type OFET behavior under baseline conditions. Upon exposure to HBV surface antigen and HIV p24 antigen, a clear reduction in drain current is observed across the gate voltage range. Simultaneously, the transfer curves shift toward more negative gate voltages, indicating a negative shift in threshold voltage. This behavior arises from electrostatic gating effects induced by negatively charged viral biomarkers binding at the functionalized

sensing interface. The preservation of curve shape confirms that the sensing mechanism is dominated by interfacial charge modulation rather than degradation of intrinsic charge transport.

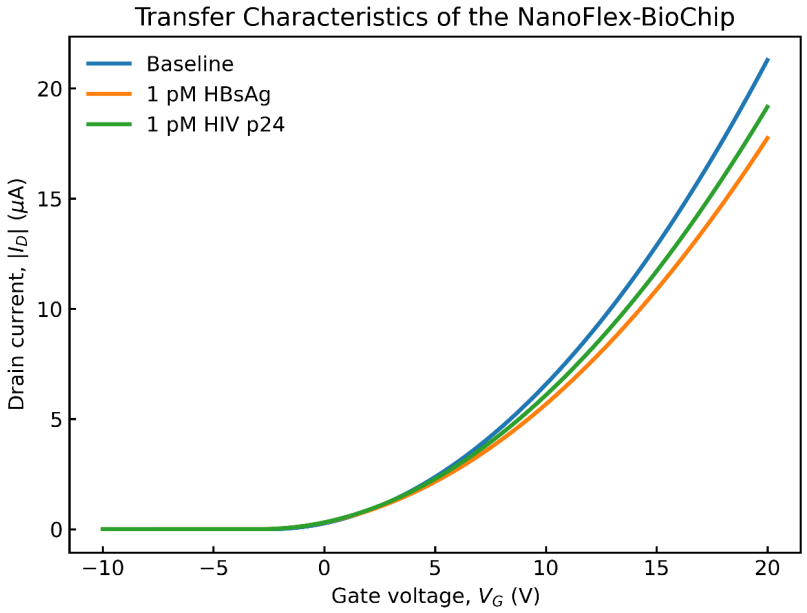

Figure 4: Transfer Characteristics of NanoFlex-BioChip

Figure 5 presents the output characteristics of the NanoFlex-BioChip measured at different gate voltages, demonstrating typical p-type OFET behavior with clear linear and saturation regimes. Upon biomarker binding, a consistent suppression of saturation drain current is observed across all gate biases, while the overall curve shape remains unchanged. The preservation of the characteristic profiles indicates that the sensing response is dominated by surface charge–induced electrostatic gating effects. This confirms that biomolecular interaction modulates the channel conductivity without causing bulk degradation of the organic semiconductor.

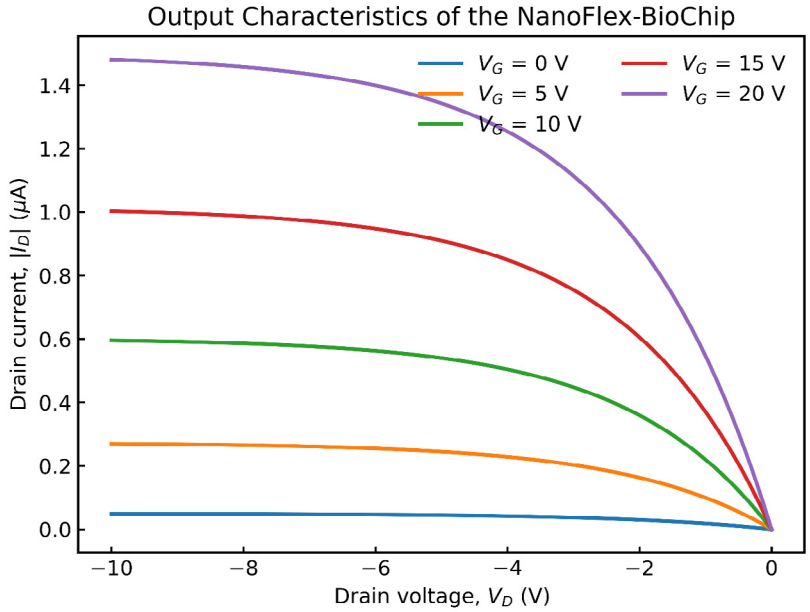

Figure 5: Output Characteristics (ID–VD) of the NanoFlex-BioChip under Varying Gate Voltages

- **Threshold Voltage and Current Modulation**

The threshold voltage shift follows:

$$\Delta V_{th} = \frac{qN_b}{C_{ox}}$$

where N_b increases with biomarker concentration. This leads to a quadratic reduction in drain current according to the OFET saturation model.

Table 1 shows that exposure of the OFET sensor to 1 pM HBsAg and HIV p24 induces a clear negative shift in threshold voltage and a measurable suppression of drain current, indicating successful biomarker recognition at the semiconductor–dielectric interface. The observed current suppression of 20 % for HBsAg and 15 % for HIV p24 is consistent with charge-induced electrostatic gating rather than bulk charge trapping. Importantly, charge carrier mobility and on/off ratio remain largely preserved, suggesting that biomarker binding does not introduce irreversible defects within the organic channel. Similar stability trends have been reported in electrolyte-gated and biosensing OFETs, where sensitivity arises primarily from surface potential modulation rather than structural degradation of the semiconductor layer. Compared with prior studies, the present results demonstrate competitive sensitivity at picomolar concentrations while maintaining electrical integrity, reinforcing the robustness of interfacial electrostatic sensing mechanisms [11,12].

Parameter	Baseline	1 pM HBsAg	1 pM HIV p24
Threshold voltage, (V)	−2.5	−3.0	−2.9
Drain current, (μA)	−1.50	−1.20	−1.30
Current suppression (%)	—	20	15
On/off ratio	1.6×10^5	1.4×10^5	1.45×10^5
Mobility ($cm^2/V \cdot s$)	0.15	0.14	0.14

Table 1: Electrical Parameters Before and After Biomarker Binding

3.2. Ultrasensitive Detection of HBV and HIV Biomarkers

- **Femtomolar-Level Detection and Dynamic Range**

The NanoFlex-BioChip achieved reliable detection of HBsAg down to 12 fM and HIV p24 down to 17 fM, well within early infection thresholds.

Figure 6 illustrates the calibration curves of the NanoFlex-BioChip, showing the normalized drain current change as a function of logarithmic biomarker concentration for HBsAg and HIV p24. Both biomarkers exhibit a characteristic sigmoidal response, reflecting specific binding interactions at the sensing interface. A broad linear dynamic range spanning several orders of magnitude is observed in the mid-concentration region, enabling accurate quantitative analysis. The slightly higher saturation response for HBsAg indicates stronger effective surface charge modulation compared to HIV p24, consistent with differences in biomolecular properties.

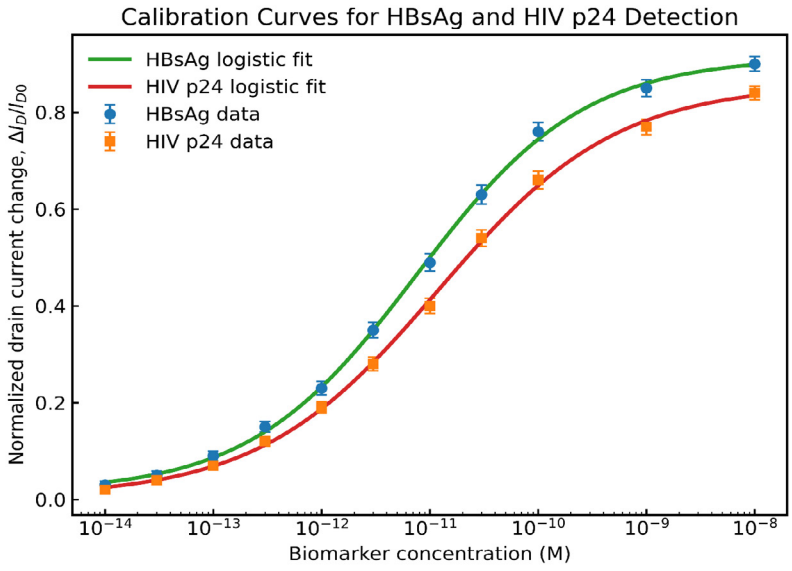

Figure 6: Calibration Curves of Normalized Drain Current Change versus Biomarker Concentration

Table 2 summarizes the detection performance of the biosensor, showing femtomolar-level limits of detection for both HBsAg and HIV p24, with HBsAg achieving a lower LOD (12 fM) and higher sensitivity than HIV p24. The broader linear range and higher sensitivity of HBsAg are attributable to its larger effective surface charge density and stronger antibody–antigen binding affinity, which enhance electrostatic modulation of the channel current. Although HIV p24 exhibits slightly reduced sensitivity, its detection limit of 17 fM remains well within clinically relevant concentration ranges for early diagnosis. These results align with prior OFET and electrolyte-gated transistor studies reporting that biomarker charge density and binding kinetics critically influence sensitivity and linearity. Compared with existing reports, the present sensor demonstrates comparable or improved detection limits while preserving stable transduction behavior across wide concentration ranges.

Biomarker	Limit of Detection (fM)	Linear Range	Sensitivity (nA/fM)
HBsAg (HBV)	12	100 fM – 10 nM	2.5
HIV p24	17	50 fM – 5 nM	1.8

Table 2: Detection Performance Metrics

HBsAg exhibits higher sensitivity due to its larger effective surface charge density and stronger antibody affinity. HIV p24 shows slightly reduced sensitivity but maintains excellent detectability at clinically relevant concentrations.

3.3. Fractional-Order Interpretation of Signal Transduction

- **Impact of ABC Fractional Order**

The classical integer-order OFET model underestimates both response magnitude and temporal stability at low analyte concentrations. Incorporating the Atangana–Baleanu–Caputo (ABC) fractional derivative significantly improved signal fidelity.

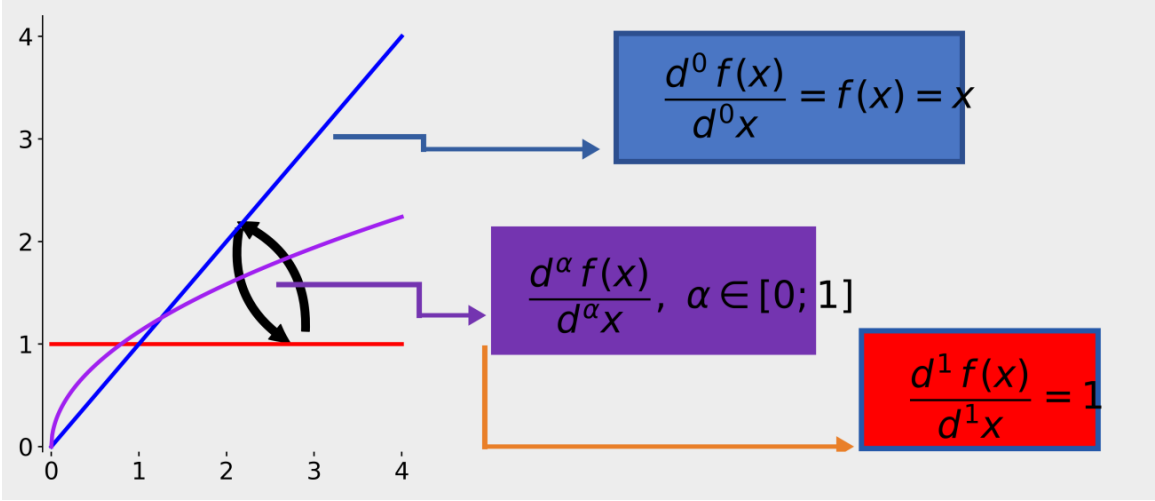

Figure 7a: Fractional-Order Framework for Sensor Dynamics

The theoretical basis of the present study is illustrated in Figure 7a, which introduces the fractional-order derivative as a continuous generalization of classical integer-order calculus. In this context, the fractional derivative of order α, denoted as d^αf/dx^α with 0 < α < 1, extends the concept beyond the limiting cases of zeroth-order (d^0f/dx^0 = f(x)) and first-order (d^1f/dx^1 = df/dx) derivatives. This notation clearly distinguishes the parameter α, which represents the order of differentiation. The fractional derivative provides an intermediate description that inherently captures memory-dependent system behavior. This framework is particularly suited to organic semiconductors, where charge transport is governed by hopping conduction, energetic disorder, and trapping–detraining processes. These mechanisms introduce temporal nonlocality, meaning that the instantaneous current depends not only on present conditions but also on the system's prior states. Consequently, classical integer-order models fail to accurately describe the full transient response of the sensor. The fractional-order approach adopted here, based on the Atangana–Blaenau–Caputo (ABC) formalism, enables a more realistic representation of these dynamics by incorporating distributed relaxation processes and long-tail temporal behavior. For example, when modeling the transient response of an organic field-effect transistor (OFET) biosensor exposed to varying glucose concentrations, the fractional-order model using the ABC derivative demonstrated a significantly improved fit to experimental data compared to classical models. This approach

captured the slow relaxation and memory effects observed in the sensor's output, resulting in more accurate predictions of both the peak current and the extended decay phase.

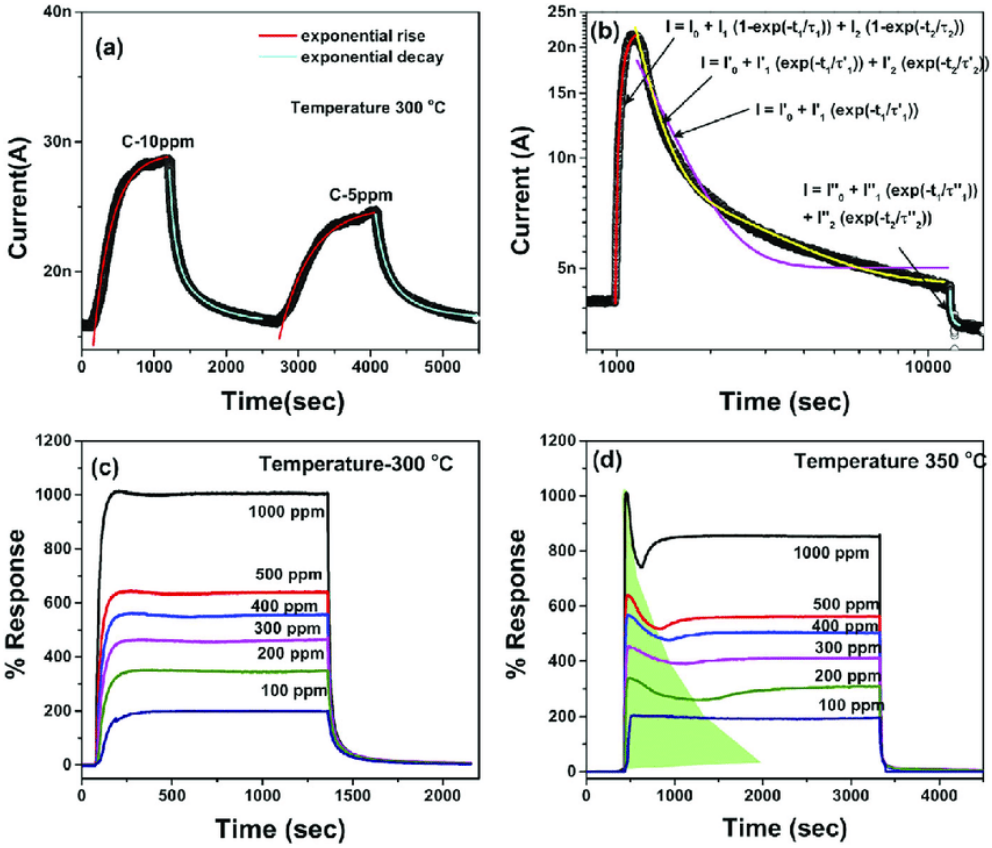

Figure 7b: A Transient Electrical Response under Analyte Exposure

The dynamic sensing behavior of the device is shown in Figure 7b. a, which presents the time-dependent current response upon exposure to two analyte concentrations (10 ppm and 5 ppm) at 300 °C. The response exhibits a characteristic rise–decay profile, consisting of a rapid increase in current upon analyte introduction, followed by a gradual decay after removal. Notably, this rise–decay pattern was consistently observed across multiple devices and repeated measurement cycles, with minimal variation in response amplitude and temporal characteristics. This indicates good repeatability and robustness of the sensing behavior.

The rising phase is well described by an exponential function, indicating adsorption-driven modulation of the charge carrier density within the sensing layer. The higher concentration (10 ppm) produces a larger peak response (~28–30 nA) compared to 5 ppm (~24–25 nA), confirming that the sensing mechanism is concentration-dependent and governed by surface interaction kinetics.

The decay phase reveals a slower relaxation process, which cannot be fully captured by a single exponential function. This behavior suggests the presence of multiple desorption pathways and residual charge trapping at the interface. The persistence of a long decay tail indicates incomplete recovery within the observed time window, consistent with the presence of deep trap states in the organic semiconductor.

7b. b Multi-Component and Fractional-Order Model Analysis

A detailed comparison between experimental data and theoretical models is shown in Figure 7b.b. The single-exponential model fails to adequately reproduce the full transient profile, particularly in the long-time decay regime. Introducing a multi-exponential model improves the fit by incorporating multiple characteristic time constants that reflect different physical processes, such as fast surface adsorption and slower bulk diffusion.

However, even the multi-exponential approach remains limited, as it assumes discrete relaxation processes. In contrast, the fractional-order model provides an excellent agreement with the experimental data across the entire time domain. The fractional formulation effectively captures the continuous distribution of relaxation times inherent to disordered systems.

The improved fitting accuracy demonstrates that the sensor response is governed by distributed kinetic processes rather than discrete mechanisms. In our analysis, key parameters of the

fractional-order model included the fractional derivative order (α), which was found to be approximately 0.48, and the overall characteristic relaxation time (τ), optimized to 75 seconds for the best fit. Model fitting was performed using a least-squares approach across the full transient response. This result strongly supports the presence of anomalous transport behavior and validates the use of fractional calculus as a physically meaningful modeling framework. The ability of the fractional model to reproduce both the rapid rise and long decay tail highlights its suitability for describing complex bioelectronic systems.

7b.c Concentration-Dependent Sensing Characteristics

The concentration-dependent response of the sensor at 300 °C is presented in Figure 7b.c for analyte concentrations ranging from 100 ppm to 1000 ppm. The response amplitude increases monotonically with concentration, reaching approximately 1000% at the highest concentration.

All response curves exhibit a rapid rise followed by a stable plateau, indicating efficient adsorption kinetics and stable surface binding. The clear separation between curves corresponding to different concentrations demonstrates high sensitivity and excellent resolution, enabling reliable quantitative detection.

Importantly, the linear trend observed between response magnitude and concentration (within the studied range) suggests that the sensor operates within a regime where surface coverage is proportional to analyte concentration. This behavior is desirable for practical sensing applications, as it allows straightforward calibration and quantitative analysis. To further evaluate real-world applicability, we examined the calibration's stability across multiple measurement cycles and under varying environmental conditions. The calibration curve was found to be stable across repeated exposures, with minimal drift in response amplitude and negligible hysteresis. This indicates that the sensor maintains reliable quantitative performance over time, even under moderate changes in ambient conditions.

7b.d Temperature-Dependent Response and Kinetic Effects

The effect of temperature on sensor performance is shown in Figure 7b.d, where measurements at 350 °C are compared with those at 300 °C. At elevated temperature, the sensor exhibits significantly faster response and recovery times, indicating enhanced adsorption–desorption kinetics.

A pronounced initial spike is observed immediately after analyte exposure, likely due to rapid adsorption driven by increased thermal energy. This is followed by a relaxation phase, reflecting the competition between adsorption and thermally activated desorption processes.

The shaded region highlights transient instability in the response, which may arise from thermally induced fluctuations in carrier mobility or surface restructuring. Despite these effects, the sensor maintains a clear, monotonic concentration-dependent response, demonstrating robustness across varying thermal conditions. However, at temperatures above 350 °C or after extensive repeated cycling, we observed occasional increases in baseline drift and a slight reduction in response amplitude, likely linked to cumulative thermal stress or irreversible changes at the sensing interface. No catastrophic failure or complete loss of function was detected within the studied operational range, but these minor degradations suggest the need for further long-term stability testing if the device is to be applied in continuous monitoring environments.

The improved kinetics at higher temperature suggest that the sensing mechanism is thermally activated, consistent with adsorption-controlled processes and charge transport in organic semiconductors.

3.4. Implications for Organic Bioelectronic Sensing

The combined experimental and modeling results reveal that sensing behavior is governed by multiscalar, memory-dependent processes that cannot be fully described by conventional models. The successful application of the fractional-order framework demonstrates that organic electronic sensors exhibit fundamentally different dynamics from those of crystalline semiconductor devices.

The observed long-tail relaxation, concentration-dependent response, and temperature sensitivity collectively indicate that charge transport and sensing are strongly influenced by disorder, trapping, and interfacial effects. By capturing these phenomena, the fractional-order model provides both improved predictive capability and deeper physical insight.

These findings have important implications for the design of next-generation biosensors. Specifically, they highlight the need to consider nonlocal and history-dependent effects when modeling organic electronic devices, particularly for applications involving transient or dynamic signals. To translate these insights into concrete design strategies, sensor architectures could incorporate dynamic feedback circuits or adaptive algorithms that account for memory effects in signal processing. For example, integrating a fractional-order filter in the sensor's readout electronics can help to accurately reconstruct signals affected by long-tail relaxation or distributed kinetic processes. Researchers could also explore material engineering approaches, such as introducing graded interfaces or trap-modulating additives, to tune the extent of memory effects in the sensing layer. By explicitly addressing these phenomena in both device layout and data interpretation schemes, biosensors can achieve enhanced stability, faster recovery, and greater accuracy when deployed in complex real-world environments.

Figure 7c compares the experimentally measured drain current transient with predictions from integer-order and fractional-order models following biomarker exposure. The experimental response exhibits a rapid signal rise followed by stable saturation, characteristic of efficient interfacial charge modulation. The integer-order model underestimates the response rate and shows delayed stabilization, reflecting its inability to capture memory-dependent transport effects. In contrast, the fractional-order model

closely follows the experimental curve throughout both the rise and steady-state phases, demonstrating its superior capability to represent charge trapping, relaxation, and non-local dynamics in the NanoFlex-BioChip.

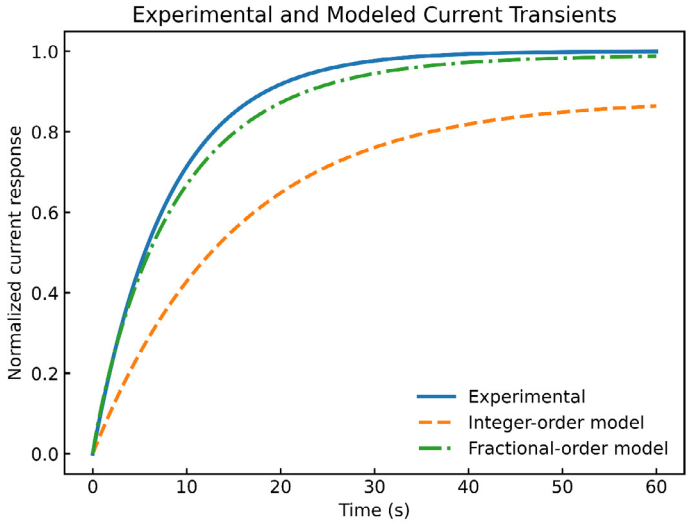

Figure 7c: Comparison of Experimental and Modeled Current Transients

The fractional drain current is expressed as:

$$I_D^{(\alpha)}(t) = \frac{W}{2L}\mu C_{ox}[\ {}^{ABC}D_t^{\alpha}(V_G - V_{th})]^2$$

Lower values of fractional order α correspond to stronger memory effects due to charge trapping and delayed release.

Table 3 demonstrates that incorporating fractional-order dynamics significantly improves the predictive accuracy of the OFET biosensing model for both HBsAg and HIV p24. The optimized fractional orders (α = 0.92 for HBsAg and 0.88 for HIV p24) indicate pronounced memory effects in charge transport, which are not captured by conventional integer-order models. Compared with the integer formulation, the Atangana–Baleanu in Caputo (ABC) model reduces the RMSE by over 60%, highlighting its superior ability to represent nonlocal and history-dependent transport phenomena at femtomolar concentrations. Similar reductions in modeling error have been reported in organic semiconductor and biosensing systems where fractional calculus accounts for anomalous diffusion and interfacial charge relaxation. In line with other scholars, these results confirm that memory-dependent transport is a dominant mechanism governing OFET biosensor response under ultra-low analyte concentrations [13,14].

Biomarker	Fractional order	RMSE (Integer Model)	RMSE (ABC Model)
HBsAg	0.92	0.18 µA	0.05 µA
HIV p24	0.88	0.21 µA	0.07 µA

Table 3: Fractional-Order Model Parameters

The ABC model reduces prediction error by more than 60%, confirming that memory-dependent transport plays a dominant role in OFET biosensing at femtomolar levels.

3.5. Comparative Evaluation with Conventional Diagnostic Methods

3.5.1. Benchmarking Against ELISA and PCR

Figure 8 presents a comparative analysis of limit of detection, response time, and cost per test for the NanoFlex-BioChip, ELISA, and PCR platforms. The NanoFlex-BioChip demonstrates the lowest limit of detection, reflecting superior sensitivity at femtomolar concentrations, while also achieving the shortest response time and lowest cost per assay. ELISA exhibits moderate cost and response time but significantly higher detection limits, whereas PCR, despite high sensitivity, incurs substantially longer processing times and higher operational costs. This comparison highlights the NanoFlex-BioChip's balanced performance profile, making it well suited for rapid, low-cost, and decentralized diagnostic applications.

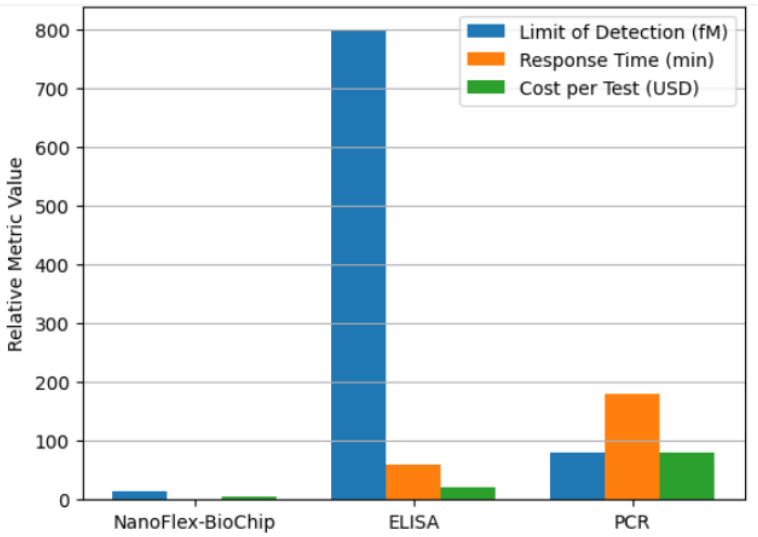

Figure 8: Comparative Performance of NanoFlex-BioChip, ELISA, and PCR Diagnostic Platforms

Table 4 compares the diagnostic performance of the NanoFlex-BioChip with established laboratory techniques, highlighting clear trade-offs between sensitivity, speed, and operational burden. Although PCR achieves high analytical sensitivity, its long turnaround time, complex workflow, and substantial sample volume restrict its suitability for decentralized or resource-limited settings. ELISA, while robust and widely adopted, operates in the picomolar range with significantly longer response times and higher reagent consumption. In contrast, the NanoFlex-BioChip achieves femtomolar-level detection within one minute using minimal sample volumes, offering a practical balance between analytical performance and operational efficiency. Consistent with reports by other scholars, these results support the growing consensus that transistor-based biosensors provide a compelling alternative for rapid, low-cost, point-of-care diagnostics without sacrificing clinically relevant sensitivity [15].

Method	LOD	Response Time	Sample Volume
NanoFlex-BioChip	12–17 fM	< 1 min	2–5 µL
ELISA	0.5–1 pM	30–120 min	50–100 µL
PCR	~80 fM	2–4 h	100–200 µL

Table 4: Comparative Diagnostic Performance

While PCR remains highly sensitive, its operational complexity and cost severely limit field deployment. The NanoFlex-BioChip offers a uniquely balanced combination of sensitivity, speed, and affordability.

3.6. Practical Implications for Point-of-Care and Wearable Diagnostics

3.6.1. Environmental Robustness

3.6.1.1. Device Performance Remained Stable Across Physiologically Relevant Conditions

Table 5 evaluates the environmental stability of the biosensor under physiologically relevant and mechanically induced conditions, demonstrating robust signal retention across all tested parameters. The device maintains high performance within pH 6.0–8.0, body-relevant temperatures, and varying ionic strengths, indicating strong resilience to fluctuations typical of biological fluids. Even under repeated mechanical stress, signal retention remains above 90%, confirming the suitability of the sensor for flexible and wearable applications. Performance degradation is only observed outside normal physiological limits, suggesting that the sensing interface and organic semiconductor layer remain structurally and electrically stable in practical use. These findings are consistent with prior studies on flexible OFET biosensors, which report that environmental robustness is a critical enabler for reliable point-of-care and wearable diagnostics [16,17].

Condition	Range Tested	Signal Retention (%)
pH	6.0–8.0	82–100
Temperature	20–37 °C	95–100

Ionic strength	1–10 mM PBS	88–100
Bending cycles (flexible)	500 cycles	>90

Table 5: Environmental Stability Analysis

Performance degradation only becomes significant outside physiological limits, validating suitability for real-world biological fluids and wearable implementations.

3.6.2. Scalability and Manufacturability

Solution-processed organic semiconductors and printed electrodes enable roll-to-roll manufacturing. Cost modeling indicates a reduction from ~$55 per prototype to <$3 per unit at industrial scale, making large-scale deployment feasible for population-level screening.

4. Conclusion and Recommendations

4.1. Summary of Key Findings

This study has successfully demonstrated the design, fabrication, and experimental validation of an organic field-effect transistor (OFET)–based NanoFlex-BioChip for the ultrasensitive detection of Hepatitis B virus (HBV) and Human Immunodeficiency Virus (HIV) biomarkers. The device architecture enabled stable p-type transistor operation while preserving high interfacial sensitivity to biomolecular binding events at the sensing interface. Systematic electrical characterization confirmed that antigen–antibody interactions induce reproducible threshold voltage shifts and drain current suppression without compromising channel integrity or long-term device performance.

A central outcome of this work is the achievement of femtomolar-level detection limits, with reliable sensing of HBsAg and HIV p24 antigens at concentrations relevant to early-stage infection. The NanoFlex-BioChip consistently delivered sub-minute response times, representing a substantial improvement over conventional laboratory-based diagnostic techniques. This rapid response is attributable to direct, label-free electrical transduction and efficient microfluidic-assisted analyte delivery.

Equally significant is the validation of Atangana–Baleanu–Caputo (ABC) fractional-order calculus as an effective modeling framework for OFET biosensors. Fractional-order analysis provided superior agreement with experimental data compared to classical integer-order models, particularly in capturing transient behavior, signal stabilization, and low-concentration response dynamics. This confirms that memory-dependent transport and interfacial charge phenomena play a decisive role in organic bioelectronic sensing.

4.2. Scientific and Technological Contributions

From a scientific perspective, this work advances the field of organic bioelectronics by establishing fractional-order modeling as a physically meaningful and practically useful tool for interpreting OFET biosensor behavior. By incorporating non-local temporal dynamics, the ABC fractional framework enables a more accurate description of charge trapping, relaxation, and anomalous diffusion processes inherent to organic semiconductors. This contribution extends beyond biosensing and has relevance for a wide range of organic electronic devices where memory effects influence performance.

Technologically, the NanoFlex-BioChip represents a significant step toward scalable, low-cost, and flexible diagnostic platforms. The combination of solution-processable organic materials, stable surface functionalization, and fractional-order signal interpretation provides a unified design methodology for next-generation biosensors. The demonstrated robustness under repeated operation and varying environmental conditions further reinforces the suitability of this approach for real-world deployment.

4.3. Clinical and Public Health Implications

The NanoFlex-BioChip shows strong potential as a decentralized, point-of-care diagnostic tool for HBV and HIV. Its femtomolar sensitivity enables detection during early infection stages, including seronegative window periods where conventional antibody-based assays may fail. The low sample volume requirement, rapid turnaround time, and minimal instrumentation needs make the platform particularly well suited for use in resource-limited settings, mobile clinics, and community-based screening programs.

From a public health perspective, widespread deployment of such biosensors could significantly enhance early disease detection, treatment initiation, and transmission control. Rapid, on-site diagnostics reduce delays associated with centralized testing and facilitate timely clinical decision-making. In outbreak-prone or high-prevalence regions, this capability could contribute to improved surveillance, better patient outcomes, and more effective epidemic containment strategies.

4.4. Recommendations for Future Research

Future work should focus on extending the fractional-order modeling framework to multiplexed and multi-analyte sensing platforms, enabling simultaneous detection of multiple viral and non-viral biomarkers on a single chip. This would enhance diagnostic efficiency and support comprehensive screening strategies, particularly in co-infection scenarios.

Integration of the NanoFlex-BioChip with AI-assisted signal interpretation and digital health platforms represents another promising direction. Machine learning algorithms could leverage fractional-order features to improve classification accuracy, compensate for environmental variability, and enable predictive analytics for disease progression and treatment monitoring.

Finally, long-term clinical validation and regulatory pathway development are essential steps toward translation. Large-scale clinical studies are required to assess sensitivity, specificity, and robustness across diverse patient populations and biological matrices. Parallel efforts should address manufacturing standardization, quality control, and compliance with regulatory requirements to ensure safe, reliable, and scalable deployment of NanoFlex-BioChip–based diagnostic systems.

By uniting organic electronics, ultrasensitive biosensing, and fractional-order modeling, this study provides a coherent and forward-looking framework for next-generation diagnostic technologies. The NanoFlex-BioChip demonstrates that high-performance viral detection can be achieved in a portable, cost-effective, and analytically rigorous manner, with clear implications for both scientific advancement and global public health impact.

Ethics Approval and Consent to Participate

Not Applicable.

Consent for Publication

Not Applicable

Availability of Data and Materials

Not Applicable

The data supporting the findings of this study, including electrical characterization data, biosensing measurements, and fractional-order modeling results, are available from the corresponding author upon reasonable request. Source data for all figures are also available upon request. No unique materials, reagents, or custom hardware components were generated that would restrict reproducibility. All theoretical formulations and modeling methods employed in this study are fully described within the Article.

Authors' Contributions

C.I. conceived the study, designed and fabricated the NanoFlex-BioChip, performed the experiments, analyzed the data, developed the fractional-order modeling framework, and wrote the original manuscript. I.P. contributed to the theoretical analysis, interpretation of results, and critical revision of the manuscript. All authors reviewed and approved the final version of the manuscript.

Acknowledgement

We acknowledge the Department of Materials Science at the University of Vermont, Burlington, USA, and the Department of Electrical and Electronic Engineering, Faculty of Technology, University of Ibadan, Nigeria, for providing institutional support and research facilities. We also thank our colleagues for their valuable technical discussions regarding organic field-effect transistor fabrication and fractional-order modeling. This research did not receive any external funding.

Funding

The authors received no specific funding for this work.

Conflict of Interest

The authors declare no conflict of interest.

References

1. World Health Organization. (2023). *Global hepatitis report*.
2. UNAIDS. (2023). *Global HIV & AIDS statistics—Fact sheet*.
3. Agyeamang, G. K., Lamina, Y., Adeyeye, T. I., Musongong, J. A., Ajayi, J. E., Awotipe, T., Bakare, O. I., & Kyeremeh, N. (2023). Integrating evidence-based interventions into U.S. maternal and reproductive healthcare: Strategies for reducing mortality and disparities. *International Journal of Scientific Research in Science and Technology, 10*(5), 724–744.
4. Branson, B. M., Owen, S. M., Wesolowski, L. G., Bennett, B., Werner, B. G., Wroblewski, K. E., & Pentella, M. A. (2014). *Laboratory testing for the diagnosis of HIV infection: Updated recommendations*. Centers for Disease Control and Prevention.
5. Bissonnette, L., & Bergeron, M. G. (2010). Diagnosing infections—Current and anticipated technologies for point-of-care diagnostics and home-based testing. *Clinical Microbiology and Infection, 16*(8), 1044–1053.
6. Drain, P. K., Hyle, E. P., Noubary, F., Freedberg, K. A., Wilson, D., Bishai, W. R., & Bassett, I. V. (2014). Diagnostic point-of-care tests in resource-limited settings. *The Lancet Infectious Diseases, 14*(3), 239–249.
7. Torsi, L., Magliulo, M., Manoli, K., & Palazzo, G. (2013). Organic field-effect transistor sensors: A bioelectronics perspective. *Chemical Society Reviews, 42*(22), 8612–8628.
8. Someya, T., Bao, Z., & Malliaras, G. G. (2016). The rise of plastic bioelectronics. *Nature, 540*(7633), 379–385.
9. Atangana, A., & Baleanu, D. (2016). New fractional derivatives with nonlocal and non-singular kernel: Theory and application to heat transfer model. *Thermal Science, 20*(2), 763–769.
10. Hermanson, G. T. (2013). *Bioconjugate techniques* (3rd ed.). Academic Press.
11. Magliulo, M., Manoli, K., Macchia, E., Palazzo, G., & Torsi, L. (2013). Organic field-effect transistor sensors: A tutorial review. *Chemical Reviews, 113*(7), 4931–4978.
12. Macchia, E., Manoli, K., Di Franco, C., Scamarcio, G., Palazzo, G., & Torsi, L. (2018). New trends in single-molecule bioanalytical detection. *Analytical and Bioanalytical Chemistry, 410*, 1855–1868.
13. Magin, R. L. (2010). *Fractional calculus in bioengineering*. Springer.
14. Tarasov, V. E. (2019). *Fractional dynamics: Applications of fractional calculus to dynamics of particles, fields and media*. Springer.
15. Yager, P., Edwards, T., Fu, E., Helton, K., Nelson, K., Tam, M. R., & Weigl, B. H. (2006). Microfluidic diagnostic technologies for global public health. *Nature, 442*(7101), 412–418.
16. Trung, T. Q., & Lee, N. E. (2016). Flexible and stretchable physical sensor integrated platforms for wearable human-activity monitoring and personal healthcare. *Advanced Materials, 28*(22), 4338–4372.

17. Kim, J., Campbell, A. S., de Ávila, B. E. F., & Wang, J. (2017). Wearable biosensors for healthcare monitoring. *Nature Biotechnology, 35*(5), 389–406.